Monthly Notices of the ROYAL ASTRONOMICAL SOCIETY

MNRAS **472,** 2410–2421 (2017) doi:10.1093/mnras/stx2112
Advance Access publication 2017 August 17

Alignments of parity even/odd-only multipoles in CMB

Pavan K. Aluri,[1]★ John P. Ralston[2] and Amanda Weltman[1,3,4]

[1]*Cosmology & Gravity Group, Department of Mathematics and Applied Mathematics, University of Cape Town, Rondebosch 7700, South Africa*
[2]*Department of Physics and Astronomy, University of Kansas, Lawrence, KS 66045, USA*
[3]*Institute for Advanced Study, Princeton, NJ 08540, USA*
[4]*Center for Computational Astrophysics, Flatiron Institute, 162 Fifth Avenue, New York, NY 10010, USA*

Accepted 2017 August 11. Received 2017 August 11; in original form 2017 April 5

ABSTRACT

We compare the statistics of parity even and odd multipoles of the cosmic microwave background (CMB) sky from *Planck* full mission temperature measurements. An excess power in odd multipoles compared to even multipoles has previously been found on large angular scales. Motivated by this apparent parity asymmetry, we evaluate directional statistics associated with even compared to odd multipoles, along with their significances. Primary tools are the *Power tensor* and *Alignment tensor* statistics. We limit our analysis to the first 60 multipoles i.e. $l = [2, 61]$. We find no evidence for statistically unusual alignments of even parity multipoles. More than one independent statistic finds evidence for alignments of anisotropy axes of odd multipoles, with a significance equivalent to $\sim 2\sigma$ or more. The robustness of alignment axes is tested by making Galactic cuts and varying the multipole range. Very interestingly, the region spanned by the (a)symmetry axes is found to broadly contain other parity (a)symmetry axes previously observed in the literature.

Key words: methods: data analysis – cosmic background radiation – submillimetre: diffuse background.

1 INTRODUCTION

Many tests of symmetry of the cosmic microwave background (CMB) sky have revealed unexplained anomalies on large angular scales, namely among low multipoles. Many low multipoles are plagued with anomalous features, associated with a breakdown of isotropy, with significances that varied between different data releases (Copi, Huterer & Starkman 2004; de Oliveira-Costa et al. 2004; Eriksen et al. 2004b; Ralston & Jain 2004; Schwarz et al. 2004; Vielva et al. 2004; Land & Magueijo 2005a; Kim & Naselsky 2010; Finelli et al. 2012; Akrami et al. 2014). In some cases, the anomalies have been attributed to statistical flukes. However, they have received significant interest from the cosmology community by way of alternate or independent analyses towards understanding these peculiarities (see for example Hajian & Souradeep 2003; Bielewicz et al. 2005; Land & Magueijo 2005b; Slosar & Seljak 2005; Abramo et al. 2006; Copi et al. 2006; Cruz et al. 2006, 2007; de Oliveira-Costa & Tegmark 2006; Wiaux et al. 2006; Bernui et al. 2007; Eriksen et al. 2007; Bernui 2008; Lew 2008; Bernui 2009; Gruppuso & Burigana 2009; Gurzadyan et al. 2009; Hansen et al. 2009; Paci et al. 2010; Cruz et al. 2011; Gruppuso et al. 2011; Hansen et al. 2011; Kim & Naselsky 2011; Maris et al. 2011; Naselsky, Hansen & Kim 2011; Sarkar et al. 2011; Aluri & Jain 2012; Ben-David, Kovetz & Itzhaki 2012; Santos, Villela & Wuensche 2012; Flender & Hotchkiss 2013; Naselsky et al. 2013; Rassat & Starck 2013; Rath & Jain 2013; Bernui, Oliveira & Pereira 2014; Rassat et al. 2014; Nadathur et al. 2014; Aiola et al. 2015; Copi et al. 2015; Polastri, Gruppuso & Natoli 2015; Quartin & Notari 2015; Schwarz et al. 2016). Regardless of interpretation, the large-scale anomalies have persisted from *WMAP* to *Planck* mission data, where the science teams pursued them with no final conclusion (Bennett et al. 2011; Bennett et al. 2013; Planck Collaboration XXIII 2014; Planck Collaboration XVI 2016).

In this paper, we uncover yet another peculiarity associated with low-multipole CMB data. We compare the alignments of parity-even and parity-odd multipoles separately to explore any preferred directions associated with each. The significances of these directions point to a particular parity preference present in the data, and possible clues about their relation to other large angle CMB anomalies.

In Kim & Naselsky (2010), an anomalous point (inversion) parity asymmetry was reported to be present in CMB data at low-l. Odd multipoles of the CMB were found to have significantly more power compared to the even multipoles in the angular power spectrum from *WMAP* 7 yr data, following an earlier analysis that used *WMAP* first year data (Land & Magueijo 2005a). Let $P^{+} = \langle D_l \rangle_{\text{even-}l}$

★ E-mail: aluripavan@gmail.com

and $P^- = \langle D_l \rangle_{\text{odd-}l}$ denote mean power in even and odd multipoles, respectively, up to a chosen $l_{\max}$ in the multipole range $l = [2, l_{\max}]$. Here $D_l = l(l+1)C_l/2\pi$, and C_l is the CMB angular power spectrum. Since the power $l(l+1)C_l \sim$ constant, at low multipoles, the ratio $R(l_{\max}) = P^+/P^-$ is expected to fluctuate about '1'. However, it was found to be significantly lower than '1' with a probability-to-exceed (PTE) the observed value in data reaching a minimum of $\sim 3\sigma$ at $l_{\max} = 22$.

This was followed by other studies confirming the anomalous nature of this parity asymmetry (Gruppuso et al. 2011; Aluri & Jain 2012). In the *Planck* 2015 analysis (Planck Collaboration XVI 2016), the p-value of this asymmetry was evaluated to be 0.2–0.3 per cent at $l_{\max} = 28$, depending on the specific component separation method used to extract the CMB signal.

The directionality of this parity asymmetry was probed by Zhao (2014), where the ratio $R(l_{\max})$ and its variants were computed in different sky directions to obtain a map of the even–odd power asymmetry with a chosen $l_{\max}$. Curiously, the minimum of the odd parity excess statistic, $R(l_{\max})$, was found to occur in the direction of the CMB dipole.

Here we analyse the even and odd multipoles separately in a wider multipole range, to explore any preferred directions associated with these point parity (a)symmetry modes.

2 POWER TENSOR, POWER ENTROPY AND ALIGNMENT STATISTICS

The Power tensor is a robust diagnostic to test isotropy of CMB data (Ralston & Jain 2004; Samal et al. 2008, 2009). The CMB temperature is conventionally expanded in terms of spherical harmonics $Y_{lm}(\hat{n})$:

$$\Delta T(\hat{n}) = \sum_{l=2}^{\infty} \sum_{m=-l}^{+l} a_{lm} Y_{lm}(\hat{n}) \, . \tag{1}$$

Here a_{lm} are the spherical harmonic coefficients, $\Delta T(\hat{n})$ denotes the CMB temperature anisotropies after subtracting the monopole and dipole and $\hat{n}$ is the position vector on the dome of the sky.

In Dirac notation, the coefficients of the spherical harmonic expansion are

$$a_{lm} = \langle l, m | a(l) \rangle \, , \tag{2}$$

where $|l, m\rangle$ represent eigenstates of the angular momentum operators J^2 and J_z. Under a small rotation, the a_{lm}'s change to

$$|a(l)\rangle' = |a(l)\rangle + |\delta a(l)\rangle \, , \tag{3}$$

where the infinitesimal change is given by $|\delta a(l)\rangle = -i \boldsymbol{J} \cdot \boldsymbol{\Theta} |a(l)\rangle$. Here J_i (i = 1–3) are the angular momentum matrices in spin-l representation, and Θ_i are the angles of rotation. To find the axes along which the maximum change is achieved, compute the Hessian, which is

$$\frac{\partial}{\partial \Theta_i \partial \Theta_j} \langle \delta a(l) | \delta a(l) \rangle = \langle a(l) | J^i J^j | a(l) \rangle \equiv A_{ij} \, . \tag{4}$$

The eigenvectors of A_{ij} define the frame to which maximal change is developed under rotations. The corresponding statistic A_{ij} that we call *Power tensor* is defined as

$$A_{ij}(l) = \frac{1}{l(l+1)(2l+1)} \sum_{mm'm''} a_{lm} J^i_{mm'} J^j_{m'm''} a^*_{lm''} \, . \tag{5}$$

Under the assumption of statistical isotropy, different spherical harmonic coefficients are uncorrelated i.e. $\langle a_{lm} a^*_{l'm'} \rangle = C_l \delta_{ll'} \delta_{mm'}$, and hence $\langle A_{ij} \rangle = (C_l/3)\delta_{ij}$. Thus, in an ensemble realizations of uncorrelated, statistically isotropic CMB sky, the eigenvalues of the Power tensor are randomly distributed about the mean value of $C_l/3$. The Power tensor eigenvectors are also distributed uniformly over the sky.

Thus, Power tensor maps the complicated pattern of each multipole on the sky on to an ellipsoid whose axes lengths are given by its eigenvalues, and the three ellipsoid axes by its eigenvectors. Hence, Power tensor can be used to characterize axiality, planarity, as well as consistency with isotropy of each multipole by comparing the ratio of its eigenvalues (i.e. shape of the ellipsoid), with the corresponding eigenvector denoting the direction of isotropy breakdown.

In any given realization, the eigenvalues of the Power tensor will not be equal. Let the eigenvalues and eigenvectors corresponding to a multipole be denoted Λ_α and e^i_α, where 'α' denotes the three eigenindices and 'i' denotes the components of each eigenvector $\boldsymbol{e}_\alpha$. We also define the *principal eigenvector* (PEV) as the eigenvector associated with the largest eigenvalue. Each PEV is then taken as the anisotropy axis corresponding to a multipole l.

The significance of anisotropy/axiality represented by a PEV can be quantified using *Power entropy*, defined as

$$S = -\sum_{\alpha=1}^{3} \lambda_\alpha \ln(\lambda_\alpha) \, , \tag{6}$$

where $\lambda_\alpha = \Lambda_\alpha / \sum_\beta \Lambda_\beta$ are the normalized eigenvalues of the Power tensor. In the limit that a multipole is highly anisotropic, one normalized eigenvalue will tend to being '1'. Correspondingly, the Power entropy $S \to 0$. If statistical isotropy holds, then each normalized eigenvalue is equal to 1/3, and $S \to \ln(3) \approx 1.0986$, which is the maximum possible value.

The PEVs make it possible to compare the *orientations* of different multipoles, which a priori contain information, that is independent of the power. A typical statistic is the dot-product-squared of PEVs from two distinct multipoles l and l'. Squaring the dot product removes the arbitrary sign convention of eigenvectors.

To quantify correlations in a set of PEVs from a range $l_{\min} \le l \le l_{\max}$, we use the *Alignment tensor* $\boldsymbol{X}$, which is defined as

$$X_{ij}(l_{\min}, \, l_{\max}) = \sum_{l=l_{\min}}^{l_{\max}} \tilde{e}^i_l \tilde{e}^j_l \, , \tag{7}$$

where $\tilde{\boldsymbol{e}}_l$ is the PEV of a multipole l. Let ζ_α and $\boldsymbol{f}_\alpha$ denote the normalized eigenvalues and eigenvectors of this Alignment tensor. The eigenvalues are normalized to remove the trivial effect of the l-range. One then computes the *Alignment entropy*, S_X, which is a rotationally invariant summary of the ratios of ζ_α, that is given by

$$S_X = -\sum_{\alpha=1}^{3} \zeta_\alpha \ln(\zeta_\alpha) \, . \tag{8}$$

When the PEVs over the range are uncorrelated, $X_{ij} \sim \delta_{ij}$ and all ζ_α are equal. In the extreme opposite case when the PEVs over the set of multipoles are all parallel to a single eigenvector, then all but one $\zeta_\alpha \to 0$. That leads to the maximal range of Alignment entropy as $0 \le S_X \le \ln(3)$. The lower limit $S_X \to 0$ represents the maximum possible correlation. The upper limit $S_X \to \ln(3)$ represents the completely uncorrelated hypothesis of the standard Big Bang. We define the *collective alignment vector* of a set of multipoles as the PEV of the corresponding Alignment tensor ($\tilde{\boldsymbol{f}}_\alpha$). Its significance is assessed using Alignment entropy. The reader may refer to Ralston & Jain (2004) and Samal et al. (2008) for more details about the

Power tensor method, as well as its relation to axes inferred from other statistics viz. the angular momentum dispersion maximization (de Oliveira-Costa et al. 2004) and Maxwell's multipole vectors (Schwarz et al. 2004).

3 DESCRIPTION OF PROCEDURE AND DATA SETS

3.1 Analysis procedure

The Power tensor and Alignment tensor allow us to probe any underlying anisotropy axis associated with CMB anisotropies from a desired multipole range or a set of multipoles.

Under point inversion, $a_{lm} \rightarrow (-1)^l a_{lm}$, and so the even(odd) multipoles are symmetric(antisymmetric) under such operation. In this work, we apply the Alignment tensor statistic to even and odd multipoles separately. Thus we can explore any common preferred axes underlying these modes separately.

We first compute the PEV corresponding to each multipole in a chosen multipole range $l = [l_{\rm min}, l_{\rm max}]$. The PEVs are separated between even and odd multipoles to construct the Alignment tensor for each parity set separately. The PEV of the Alignment tensor will provide the common anisotropy axis corresponding to each set of parity even/odd multipoles under study. The significance of anisotropy represented by this axis is measured using Alignment entropy. This is done by computing the lower tail probability deduced from simulations in comparison to the observed entropy value from data. We also study alignments in cumulative multipole bins, by varying the upper and lower end of the l-range being considered.

3.2 Real and mock data used

For this study, we use the full sky `Commander` CMB map, derived from *Planck* 2015 data, that is made publicly available.[1] It is a maximum likelihood estimate of the CMB map, along with various astrophysical components such as Galactic synchrotron, thermal dust, their spectral indices, etc., that uses multi-frequency CMB observations and external observations/templates for various Galactic emission types (Eriksen et al. 2004a, 2008; Planck Collaboration IX 2016; Planck Collaboration X 2016).

The `Commander` map is available at a resolution of HEALPIX[2] $N_{\rm side} = 2048$. However, we downgrade the map to a lower resolution of $N_{\rm side} = 256$, and smooth it to have a Gaussian beam full width at half-maximum (FWHM) $= 1^\circ$ (degrees). Since we are interested in large angular scales, this is sufficient for our purposes.

We also prepare the mock data accordingly. The *Planck* collaboration has also provided sets of CMB realizations that have the appropriate instrument effects such as beam smoothing, as well as noise realizations for public use.[3] These are referred to as full focal plane (FFP) simulations. We use the FFP8 and FFP8.1 simulation sets for our purpose. The set FFP8 was an initial release that complements the *Planck* 2015 full mission data release. However due to a slight mismatch in the theoretical power spectrum of CMB used to generate these realizations, with the angular power spectrum consistent with final *Planck* 2015 cosmological parameters, the CMB realizations were updated with a new set denoted as FFP8.1 that match *Planck* 2015 cosmology (Planck Collaboration XII 2016). Hence, we use simulated CMB skies from the set FFP8.1, but will use the FFP8 realizations for noise.

Table 1. The directions corresponding to the PEVs of $l = 2, 3$ modes obtained from Power tensor statistic are listed here. These axes are headless and the quoted direction is from the upper Galactic hemisphere. These broadly point towards the CMB kinetic dipole direction $(\ell, b) = (264^\circ, 48^\circ)$ as shown in subsequent plots. They are aligned at a mere separation of $\approx 6.2^\circ$.

l	(ℓ, b)
2	$(239.8^\circ, 57.2^\circ)$
3	$(244.3^\circ, 63.0^\circ)$

The FFP simulations of CMB and noise that are provided correspond to a specific frequency channel and are not readily usable. These simulation sets do not constitute individual component separated maps corresponding to various cleaning algorithms used by *Planck* such as `Commander`, `SMICA`, etc., to obtain clean CMB maps from the raw satellite data (Planck Collaboration IX 2016). Thus, to obtain a set of realistic CMB maps, we process this ensemble of multi-channel maps as follows.

We downgrade all the CMB and noise realizations to a common resolution of HEALPIX $N_{\rm side} = 256$, and smooth to have a uniform beam resolution of FWHM $= 1^\circ$ (degrees) Gaussian beam. We apply the HEALPIX facilities `anafast`, `alteralm` and `synfast` in that order to bring them to the aforementioned common HEALPIX resolution and beam smoothing. We used the circularized beam transfer functions corresponding to each *Planck* frequency channel, that are provided with the second public release of *Planck* data. We then compute the noise rms corresponding to each channel using these smoothed/downgraded realizations. These noise rms maps are used to combine the smoothed/downgraded individual frequency specific CMB and noise realizations through inverse noise variance weighting. Thus we are considering only the diagonal part of the full covariance matrix that results from beam smoothing. However since we are interested in studying large angular scales, the co-added CMB and effective noise maps thus obtained would sufficiently represent the observed sky.

A set of 1000 CMB and noise Monte Carlo realizations are provided with appropriate instrument and noise characteristics through *Planck* public release 2. Correspondingly we generate 1000 co-added CMB maps with noise from the FFP realizations following this procedure.

4 RESULTS

We are interested in any preferred directional correlations associated with even versus odd multipoles corresponding to large angular scales of the CMB sky. We use the multipole range $l = [2, 61]$ for this study. Before proceeding we discuss the anomalous alignment of quadrupole and octopole modes of the CMB seen in *WMAP* as well as *Planck* data, that have received considerable attention [see Bennett et al. (2013) and Planck Collaboration XXIII (2014) for the assessment of the *WMAP* and *Planck* collaborations].

4.1 Quadrupole–octopole alignment

The alignment of the quadrupole ($l = 2$) and octopole ($l = 3$) anisotropy axes as seen in the *Planck* full mission `Commander`

[1] http://irsa.ipac.caltech.edu/data/Planck/release_2/all-sky-maps/matrix_cmb.html
[2] http://healpix.jpl.nasa.gov/
[3] http://crd.lbl.gov/cmb-data

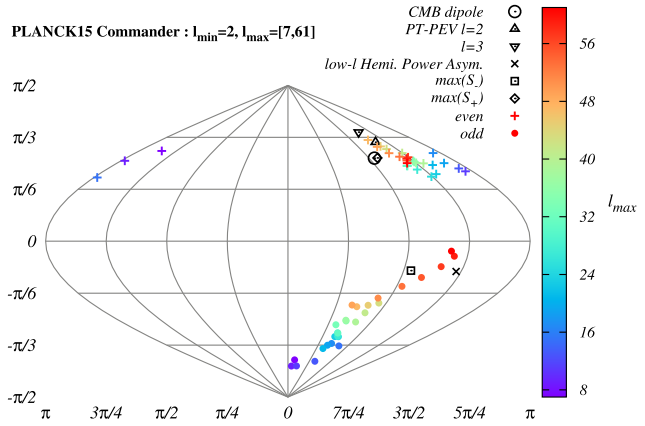

Figure 1. Collective alignment vectors, i.e. PEVs of the Alignment tensor $X(l_{\rm min}, l_{\rm max})$ (equation 7) for even and odd multipoles, obtained from *Planck* 2015 `Commander` full sky CMB map are shown here in Galactic co-ordinates. The +'s denote even-l and the •'s correspond to odd-l alignment axes. Other prominent anisotropy axes seen in the CMB sky are also labelled.

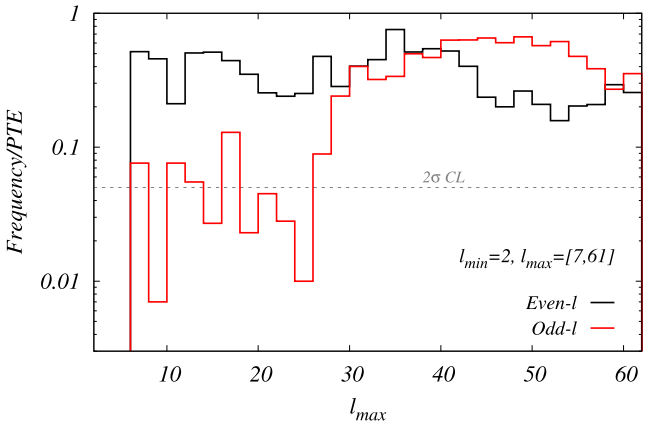

Figure 2. Significances of the collective alignment axes, shown in Fig. 1, as measured using Alignment entropy, S_X, are plotted here as a function of $l_{\rm max}$. The lower end of the multipole bin is fixed to $l_{\rm min} = 2$. The upper end of the multipole bin is varied as $l_{\rm max} = [7, 61]$. The probability to exceed the observed value of S_X from data in comparison to simulations is plotted in *black* and *red* solid curves for even and odd multipoles, respectively. We see that the odd multipole alignment axes are significantly directional at $\sim 2\sigma$ level on large angular scales.

map deserves comment. The directions inferred from the PEV corresponding to $l = 2$ and 3 multipoles are listed in Table 1. Since eigenvectors of the Power tensor are headless vectors, we report the direction of these axes from only one of the hemispheres. We find that these two modes are well aligned with a separation of only $\approx 6.2^\circ$. This corresponds to a random chance occurrence probability of $1 - \cos(6.2^\circ) \approx 0.0058$, which is close to a 3σ significance. Together with the CMB dipole, the quadrupole and octopole modes point towards the Virgo cluster (Ralston & Jain 2004). These axes are shown in subsequent plots as some of the reference anisotropy directions seen in the CMB sky. Note that the alignment of CMB temperature quadrupole and octopole modes was found to improve by applying any additional corrections such as residual Galactic bias correction (Aluri et al. 2011) or kinetic quadrupole correction, frequency independent (Schwarz et al. 2004) or frequency dependent (Notari & Quartin 2015). The *Planck* 2015 foreground cleaned maps have the frequency independent kinetic Doppler boost contribution subtracted (Planck Collaboration IX 2016). Here we used the *Planck*'s `Commander` 2015 CMB map as provided.

4.2 Parity alignments

Using the PEVs computed for each 'l' from the multipole range of our interest, we construct the Alignment tensor defined in equation (7) for even and odd multipoles separately.

First we present results for the case of varying $l_{\rm max}$, meaning, we fix $l_{\rm min} = 2$ and vary $l_{\rm max} = [7, 61]$. So, the smallest range considered is $l = 2$–7, and the Alignment tensor is computed separately for even and odd multipoles using $l = 2$, 4, 6 and $l = 3$, 5, 7 PEVs, respectively. Then we keep increasing the multipole range up to $l_{\rm max} = 61$ by two multipoles each time (so that there are an equal number of even and odd multipoles for computing the Alignment tensor), and obtain the common anisotropy axis for the set of even/odd multipoles in the current range every time. The results are shown in Fig. 1.

There seems to be an apparent clustering of even multipoles, denoted by +'s, broadly oriented along the CMB kinetic dipole ($l = 1$) direction. By progressively adding more multipoles to the Alignment tensor, the derived PEV moves closer to the CMB dipole direction. On the other hand, the common alignment axis of odd multipole PEVs, plotted in the same figure using • point types, steadily drifts from being close to the southern Galactic pole towards the Galactic plane.

We assess the significance of these collective alignment axes of even/odd multipoles using the Alignment entropy (S_X) defined in equation (8). The value of the Alignment entropy obtained from the data is compared with the same quantity computed from simulations. The p-value plot for the observed value of S_X as a function of $l_{\rm max}$ is shown in Fig. 2. We find that the apparent clustering indicated by the common alignment axes of even multipoles (black curve) is not significant, as the p-value curve is always within 2σ in the multipole range considered. However, it could be an indication of a remnant anisotropy (or a leakage) that is resulting in the apparent clustering of these axes towards CMB dipole.

In the same plot, Fig. 2, we also show the significances of odd multipole alignment axes as a function of $l_{\rm max}$ (red curve). We find that these axes are highly directional, despite the change in their orientation steadily with the addition of more multipoles. The significance fluctuates about the 2σ confidence level up to $l_{\rm max} = 27$, and becomes insignificant thereafter. So, by adding more multipoles, the directionality of common alignment axis of odd multipoles seen at low-l is weakened.

For reference, we also plot other interesting anisotropy directions seen in the CMB data with different point types in black. The quadrupole and octopole axes listed in Table 1 of the present analysis are denoted by up and inverted triangles, respectively. The CMB dipole direction and the low-l hemispherical power asymmetry axis, that is obtained from the analysis of *Planck* 2015 data using the BipoSH framework (Planck Collaboration XVI 2016), are highlighted using a black circle and a cross, respectively. A set of interesting anisotropy axes corresponding to a mirror parity (a)symmetry are also found in the CMB data (Planck Collaboration XVI 2016). However, only the mirror asymmetry axis is found to be anomalous. The maximum mirror symmetry axis is labelled max(S_+), and the maximum mirror asymmetry axis is labelled as max(S_-). These two axes are highlighted using a black diamond and a square, respectively in Fig. 2.

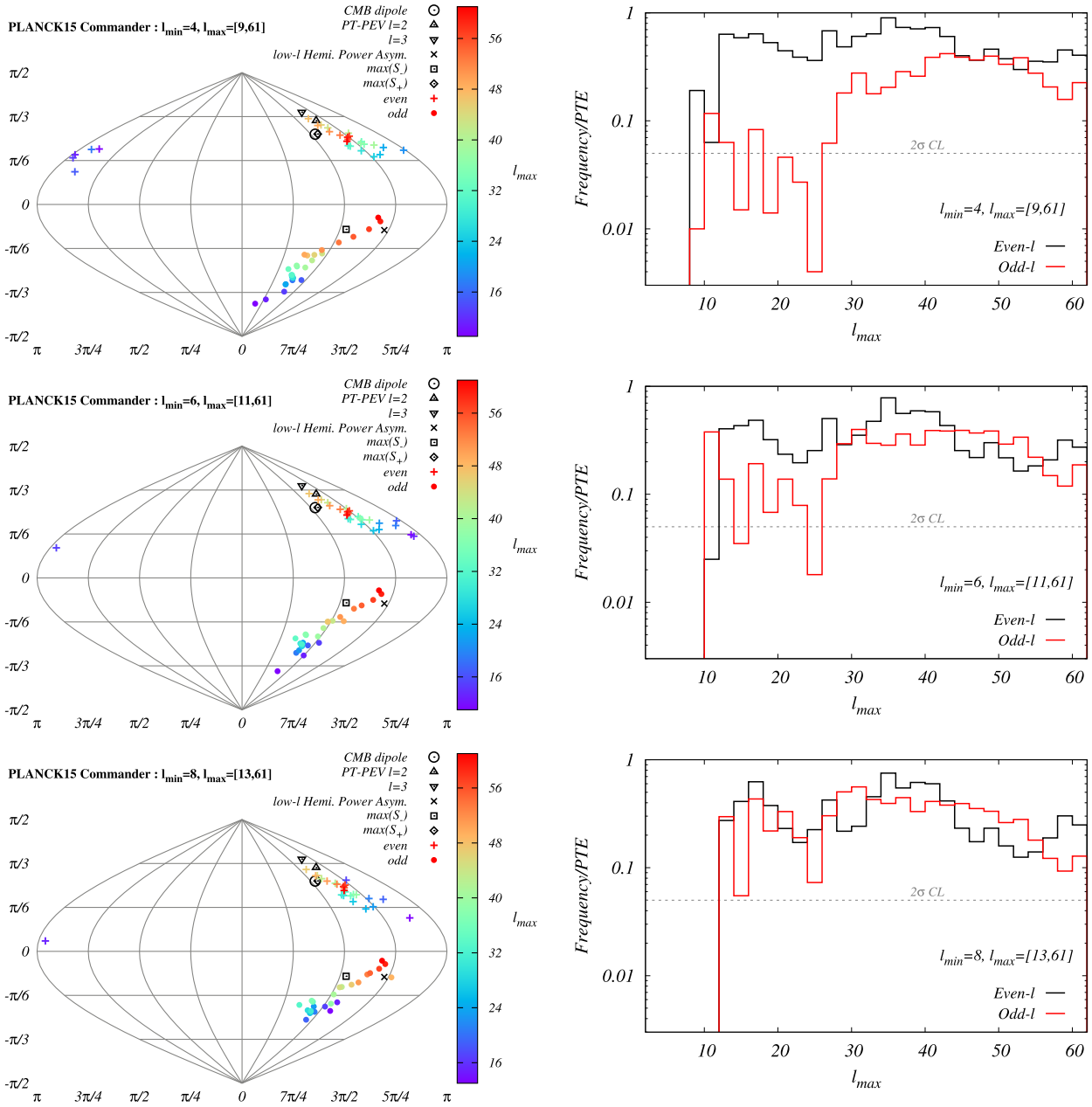

Figure 3. Same as Figs 1 and 2, but for different $l_{\rm min}$. Although the broad orientation of the axes persists by progressively excluding the first few multipoles in these plots, we find that their significances however fall (below 2σ) as seen from the *p*-value plots shown in *right-hand* column.

It is interesting to note that the even-/odd-multipole common axes span two broad regions of the sky in an apparently non-random/non-overlapping manner. One can readily see that the common alignment axes of even-multipole PEVs found here and the (insignificant) even mirror parity direction – max(S_+) are broadly aligned with the CMB kinetic dipole direction. The region spanned by the odd multipole common alignment axes contains the odd mirror parity axis – max(S_-) and the odd parity low-l dipole modulation axis.

Aluri & Jain (2012) found that the significance of the even–odd multipole power asymmetry in CMB angular power spectrum significantly decreases when the first few multipoles are omitted. We now test for low-multipole contributions to the $\sim 2\sigma$ significance seen for the directionality of odd multipole alignment axes. We repeat the calculations, while choosing different $l_{\rm min}$ values, i.e. $l_{\rm min} = 4$, 6 and 8. The results are shown in Fig. 3 in the left-hand column. We find that the distribution of common alignment axes still persists for different low-l cuts, i.e. using different $l_{\rm min}$, but varying the other end of the multipole window up to $l_{\rm max} = 61$.

However, similar to what was observed by Aluri & Jain (2012), we find that the significance of odd multipole PEV alignments quickly disappears when $l_{\rm min}$ of the multipole window is varied. The *p*-value plots corresponding to choosing different $l_{\rm min}$ are shown in the right-hand column of Fig. 3. The even-multipole alignments remain insignificant in this case as well.

To study the alignment preferences of high-l in the multipole range under consideration, we fix $l_{\rm max}$ and vary $l_{\rm min}$. In Fig. 4, we show the collective alignment axes obtained by varying $l_{\rm min}$ in

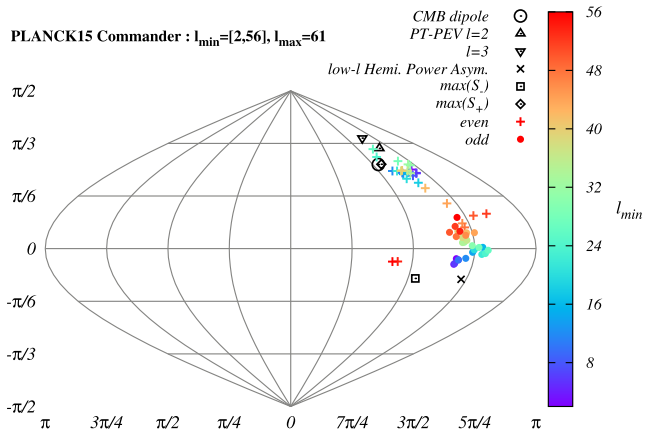

Figure 4. The alignment axis of even and odd multipole PEVs (denoted by + and •, respectively), in Galactic co-ordinates, for fixed $l_{\rm max} = 61$ and varying $l_{\rm min}$ in the range $l = [2, 56]$.

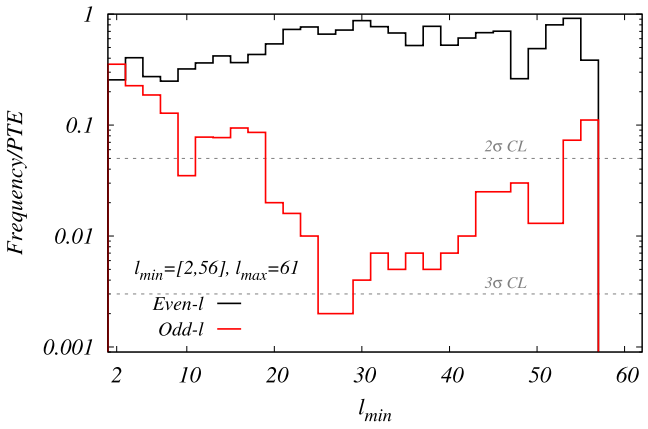

Figure 5. The lower tail probabilities or the probability to exceeed the observed Alignment entropy, S_X, of the collective alignment axes from data in comparison to 1000 simulations as a function of $l_{\rm min} = [2, 56]$, while fixing $l_{\rm max} = 61$ are shown here. The significances of observed S_X of even and odd multipole common anisotropy axes are plotted in *black* and *red* solid curves, respectively.

the range $l = [2, 56]$, with fixed $l_{\rm max} = 61$. The significance of these axes as a function of $l_{\rm min}$ is plotted in Fig. 5. This study suggests a possibility of two distinct populations for $l \lesssim 30$ compared to $30 \lesssim l \leq 61$ when contrasted with varying $l_{\rm max}$ case. We find a $\sim 2\sigma$ significance up to $l_{\rm max} \sim 30$ in the varying $l_{\rm max}$ case. However in the varying $l_{\rm min}$ case, the significance keeps building up up to $l_{\rm min} \sim 30$, which indicates two distinct populations of anisotropy axes.

We observe the alignment axis of even-multipole PEVs drifting towards the Galactic plane as more and more low-l are discarded. In comparison, the odd multipole PEVs' alignment axis now seems to have settled at the Galactic plane. The significance of the common alignment axis becomes acute for $l_{\rm min} \sim 28$. A residual foreground bias may explain the clustering of these axes in the Galactic plane, and also the corresponding anomalous significance. We pursue this aspect later in the paper.

Now we probe the observed clustering of common alignment axes of even-multipole PEVs further. The absolute scalar product of the common axes obtained from the smallest and largest subset of multipole bins of even/odd 'l' PEVs from the whole multipole range $l = [2, 61]$ is computed. This product denoted by $\cos(\alpha)$ is taken as representative of these axes being closer or scattered away from each other. The frequency plots of $\cos(\alpha)$ corresponding to even and odd multipoles, as obtained from simulations, are shown in Fig. 6. The two cases of varying $l_{\rm max}$ and $l_{\rm min}$ while fixing the other end of the multipole window are shown in that figure, in the *left-hand* and *right-hand* panels, respectively. The observed value of the inner product of the same axes from the data is denoted by vertical dashed lines in respective colours. From the histogram plot, we see that the clustering of even-multipole common axes is not statistically significant in both cases of varying $l_{\rm max}$ and $l_{\rm min}$. In contrast with this, the scalar product of odd-multipole common axes from the smallest and largest subsets is statistically significant in comparison to simulations.

The simulations suggest that the collective alignment axes, computed using Alignment tensor, from the smallest and largest multipole bin windows, tend to be closer to each other. This could be because the small multipole bin window is a subset of the larger multipole window, and thus correlated, leading to this preference. Upon extending the multipole window range ($l_{\rm max}$), we observe that the distributions tend towards being uniform, as expected.

We tested the stability of alignment axes by applying Galactic masks with different sky fractions, and inpainting the masked CMB maps using ISAP software[4] (Starck, Rassat & Fadili 2013). The publicly available *Planck* HFI masks were used which exclude 1 per cent, 3 per cent, 10 per cent, 20 per cent and 30 per cent of the sky fraction.[5] We find that the odd multipole alignment axes are stable up to an exclusion of 10 per cent of the sky in the Galactic plane. However, the even-multipole common axes are found to be sensitive to Galactic cuts. They progressively move towards or away from the Galactic plane in the varying $l_{\rm max}$ and $l_{\rm min}$ cases, respectively, while remaining broadly clustered. Applying a Galactic mask with 80 per cent or less, sky fraction is found to destroy the collective orientation of these axes. This analysis is presented in Appendix A.

We then tested the effect of including more multipoles by extending the multipole range to $l_{\rm max} = 71, 81, 91$ and 101. Any significant alignments seen in studying the multipole window $l = [2, 61]$ vanish. This is not unexpected, as it could be a simple consequence of diluting the signal.

Finally, we analysed clean CMB maps obtained using other cleaning procedures and data sets. We find a similar behaviour for the even-/odd-multipole common axes in *WMAP* provided 9 yr internal linear combination[6] (ILC) map (Bennett et al. 2013), and the Local-Generalized Morphological Component Analysis (LGMCA) map that was produced using both the *WMAP* and *Planck* full mission observations[7] (Bobin, Sureau & Starck 2016).

We also checked collective alignment axes in multipole blocks of $\Delta l = 6$ from the same range $l = [2, 61]$, with three even/odd multipoles in each block. The alignment axes thus inferred for even/odd multipoles accordingly span the same region, from lowest multipole bin to the highest, as seen in varying $l_{\rm max}$ and $l_{\rm min}$ cases. However, the cumulative statistics are better suited for our purpose, i.e. to probe the widest possible correlations across (even/odd) multipoles.

4.3 Dissecting cumulative statistics

The cumulative statistics do not give much information on which regions of the data dominate the analysis. The Alignment entropy is also just a single-number summary that cannot completely identify the source of this anomaly. To glean more information about the

[4] http://www.cosmostat.org/software/isap/
[5] http://irsa.ipac.caltech.edu/data/Planck/release_2/ancillary-data/
[6] https://lambda.gsfc.nasa.gov/product/map/current/
[7] http://www.cosmostat.org/product/lgmca_cmb/

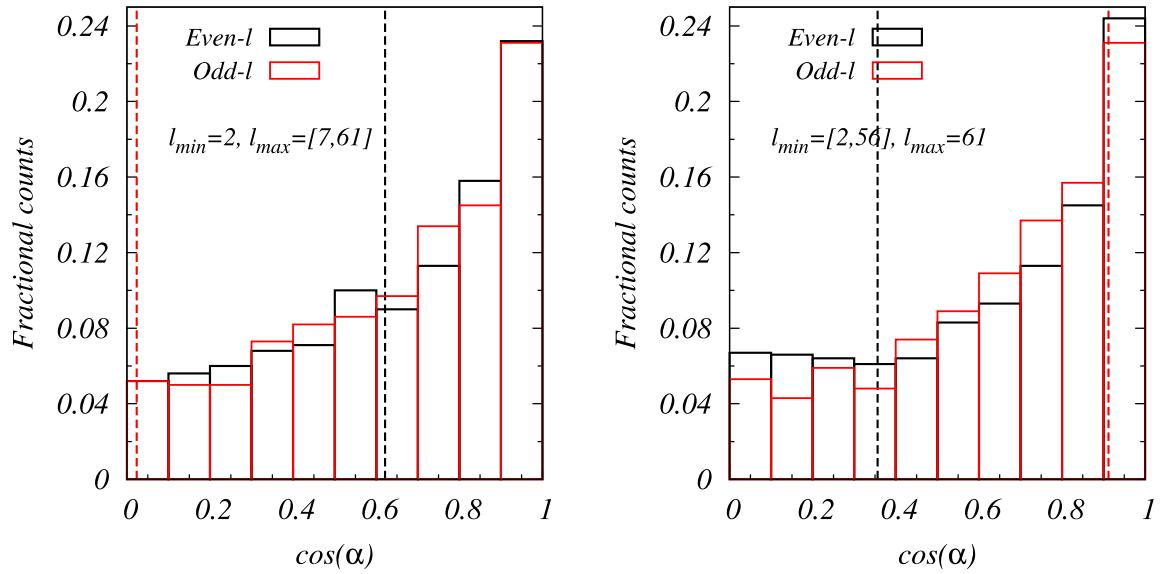

Figure 6. Distribution of the observed clustering of even- or odd-multipole PEV common axes computed as dot products of collective alignment axis from the smallest and largest multipole bin sets from the range $l = [2, 61]$. For the varying $l_{\rm max}$ case (*left-hand plot*), the inner product is taken for the axes obtained from the multipole bins $l = [2, 7]$ and $l = [2, 61]$. The varying $l_{\rm min}$ case (*right-hand plot*) uses common alignment axes obtained from the Alignment tensor for the bins $l = [2, 61]$ and $l = [56, 61]$. The scalar product of collective alignment axes corresponding to smallest and largest bins of even/odd multipoles are shown in black/red colors respectively.

observed alignments, we look inside the cumulative statistics in this section, while also introducing an *independent* statistic for testing isotropy.

To make a more informative statistic from PEVs $|\tilde{e}_l\rangle$, we first observe that normalized eigenvectors are equivalent to rank-1 projection operators $\Pi_l = |\tilde{e}_l\rangle\langle\tilde{e}_l|$. We can then define a *Hilbert–Schmidt* inner product (HSIP) (Reed & Simon 1972) as

$$B_{ll'} = Tr\{\Pi_l^\dagger \Pi_{l'}\} = \langle\tilde{e}_l|\tilde{e}_{l'}\rangle^2. \quad (9)$$

For a set of 'n' unit vectors, there will be a total of '$n(n-1)/2$' such independent inner products possible. The distribution of these independent HSIPs treated as a random variable, $B_{ll'} \to x$ (for all l, and $l' < l$), has an analytic form given by $f(x) = 1/(2\sqrt{x})$ for $0 \leq x \leq 1$ (see Appendix B for details). Correspondingly, its cumulative distribution function is given by $F(x) = \sqrt{x}$. We refer to the analytic isotropic null distribution function as *aPDF*, and the corresponding cumulative distribution function as *aCDF*. Analogously, we refer to the empirical counterparts as *ePDF* and *eCDF*, respectively. The aPDF in this form is normalized to have unit area under the curve.

Before proceeding further we first check that $f(x) = 1/(2\sqrt{x})$ is the true PDF of HSIPs of isotropically distributed unit vectors. We generate 1000 sets of $n = 30$ units vectors. All possible HSIPs among these unit vectors are computed for each set of 30 normalized vectors which will be a total of $30 \times 29/2 = 435$. Then the *mean* empirical distribution function is built by taking the average of individual ePDF histograms of 1000 sets of 30 isotropic unit vectors to compare with the analytic distribution function. The *mean* and *analytic* PDFs are shown in Fig. 7. The 435 independent HSIPs for each set of 30 isotropic unit vectors are sorted into 50 bins to compare the aPDF and ePDF. We find excellent agreement between the two distribution functions.

Now we evaluate the ePDF and eCDF of HSIPs from the data (*Planck* 2015 `Commander` map) and compare them with their analytic forms. We illustrate the distributions for three representative multipole ranges $l = [2, 25]$, $[2, 61]$ and $[26, 61]$. There are a total of 12, 30 and 18 even or odd multipole PEVs in these three sets. Thus

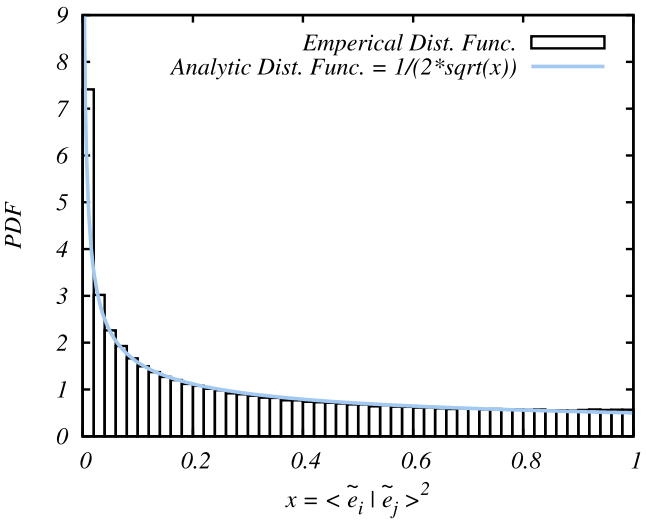

Figure 7. Test of agreement between empirical PDF of HSIP of isotropically distributed unit vectors on a sphere and their analytic distribution function. The simulation used 1000 random sets of 30 isotropically distributed unit vectors recording the ePDF histogram each time. The mean ePDF obtained from averaging individual ePDFs is shown here in bars. The analytic PDF is shown as a solid (blue) line.

$12 \times 11/2 = 66$, $30 \times 29/2 = 435$ and $18 \times 17/2 = 153$ independent HSIPs are possible, respectively, in each set of multipoles among even or odd multipole PEVs. Recall that, in the cumulative statistics, we chose the multipole range such that there are equal number of even/odd multipoles available in the l-range being considered. These are then sorted into 20 bins to build the ePDF and eCDF. The results are shown in Figs 8 and 9, for the three multipole ranges mentioned above. In describing these plots below, we only highlight a *visual* discrepancy. Later, we use *Anderson–Darling* (AD) test statistic to find whether the data conforms with the isotropic

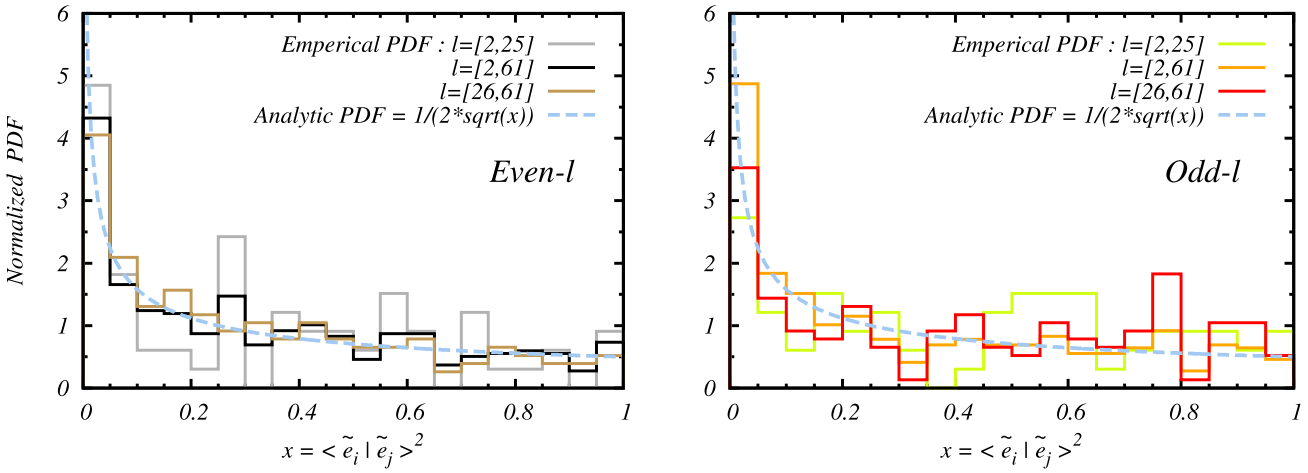

Figure 8. The empirical distribution functions of HSIPs of PEVs from data computed separately for even and odd multipoles, from three representative multipole ranges $l = [2, 25]$, [2, 61] and [26, 61] are shown here. The even and odd HSIP ePDFs are shown in *left-hand* and *right-hand* panels, respectively. The analytic distribution function is shown by a dashed (blue) line.

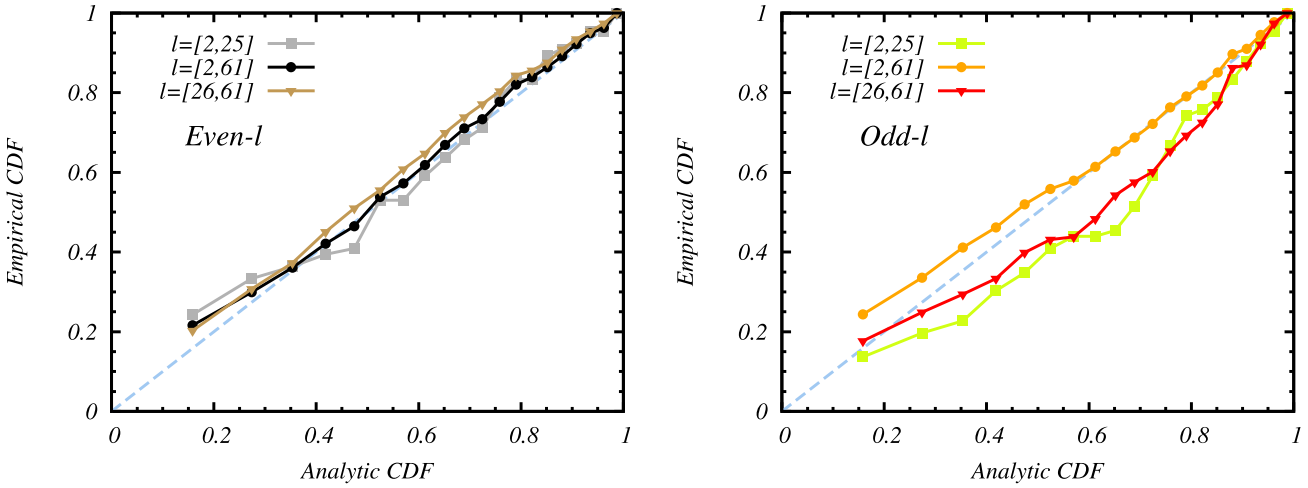

Figure 9. Same as Fig. 8, but shown here are the empirical *cumulative* distribution functions built from data HSIPs. See the text for details.

null distribution function or not, and also quantify its significance using simulations.

The eCDF plots highlight the peculiarity of odd multipole PEV alignments rather more dramatically than ePDF plots. One notices that there is a mild deficit at low-HSIP bin values, and a mild excess at intermediate HSIP bin values in the empirical PDF of odd multipole PEV alignments for the range $l = [2, 25]$ in Fig. 8. The discrepancy with the isotropic hypothesis is more striking in the empirical cumulative distribution function of odd multipole PEV HSIPs for the same range compared to the analytic distribution in Fig. 9. With larger $l_{\rm max} = 61$, the discrepancy nearly vanishes. The diagonal dashed line is the reference curve about which the data statistic coming from the null distribution is expected to fluctuate. The empirical CDF of even-multipole PEV HSIPs essentially criss-crosses this reference curve in Fig. 9, in agreement with our findings from previous sections. However, as noted above, the odd multipole alignments deviate significantly. Our earlier observation on the presence of two populations of anisotropy axes is also corroborated by the eCDF curves for $l = [2, 25]$ and $l = [26, 61]$ that are non-overlapping in multipole range.

The *AD* test (Anderson & Darling 1954; Bohm & Zech 2010) quantifies the agreement of the data with the isotropic null distribution. The AD statistic is defined as

$$AD = -N - \sum_{i=1}^{N} \frac{2i-1}{N} \left[\ln(F(x_i)) + \ln(1 - F(x_{N-i+1}))\right], \tag{10}$$

where 'N' is the number of sample points, and $F(x_i)$ is the analytic cumulative distribution function evaluated for the data sample point x_i. For our specific case of HSIPs, $F(x_i) = \sqrt{x_i}$, and for a set of 'n' even/odd multipole PEVs, there are $N = n(n-1)/2$ number of independent inner products possible. Similar to the case of varying $l_{\rm max}$ discussed in the previous section, the *AD* statistic is obtained as a function of $l_{\rm max}$ from the multipole range $l = [2, 61]$. At each $l_{\rm max}$, the *AD* statistic is computed from the even/odd multipole PEV sub sets of the current l-range separately. Likewise, we also show the results for varying $l_{\rm min}$ case.

The *AD* statistic values as a function of $l_{\rm max}$ are shown in the left-hand panel of Fig. 10, and as a function of $l_{\rm min}$ in the right-hand panel

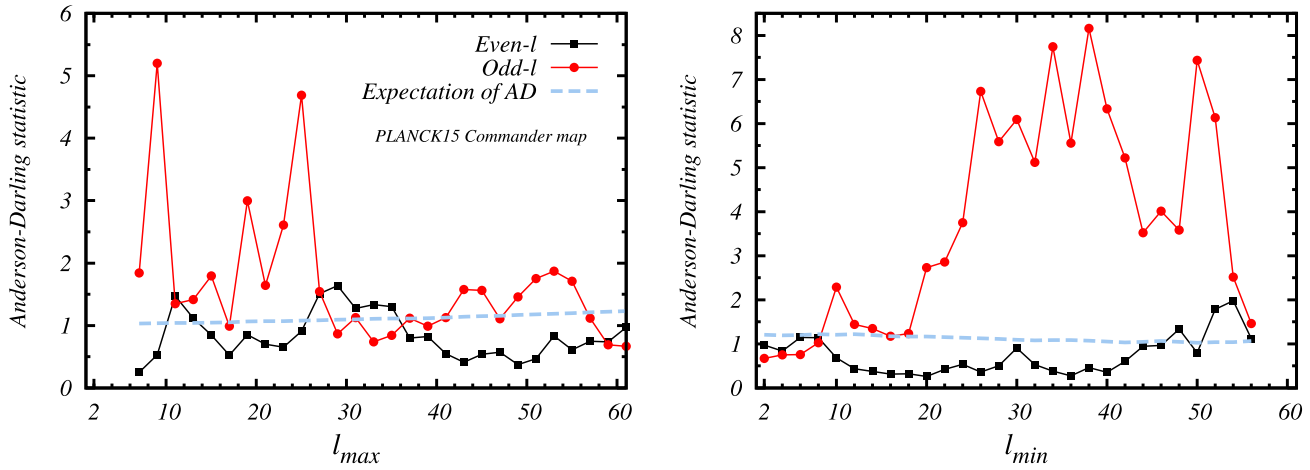

Figure 10. The AD statistic computed separately for even- and odd-multipole PEV HSIPs from *Planck* 2015 `Commnader` map are shown here. The case of varying $l_{max}(l_{min})$ are shown in *left-hand* (*right-hand*) panel. The even and odd multipole statistic values are shown in black and red solid lines with square and filled circle point types, respectively. The dashed (blue) curve denotes the expected statistic value, obtained from an ensemble of 1000 mock observed CMB maps, that is same for even or odd multipole PEVs.

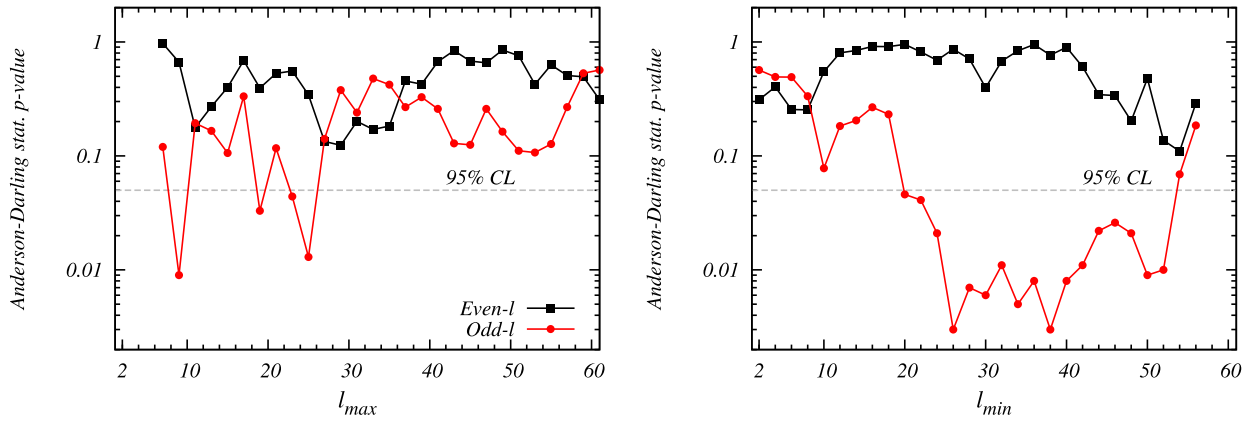

Figure 11. *p*-values of AD statistics of data shown in Fig. 10 are plotted here as a function of l_{max} and l_{min}. The significances show a similar trend for even or odd multipoles as seen with the Alignment tensor method in Figs 2 and 5. The 95 per cent confidence level is also shown for reference, as a dashed grey line in the plot. The statistic shows higher significances for $l_{max} = 9, 19, 23, 25$ indicating the possible source of the $\sim 2\sigma$ significances seen earlier, with odd multipole PEV alignments on large angular scales, in the Alignment entropy analysis.

in the same figure. The expected value of the *AD* statistic is denoted by a (blue) dashed line. It is computed from 1000 ILC-like noisy CMB maps obtained from FFP simulations described in Section 3.2. The mean *AD* statistic from simulations is evaluated in both cases for even and odd multipoles separately. Since the two curves are indistinguishable, as expected, only one of them is shown to avoid redundancy. From Fig. 10, one can readily see that the *AD* statistic for $l_{max} = 9$, 19, 23 and 25 acquires very high values, hinting at the origin of the 2σ level significance seen for the common alignment axes of odd multipole PEVs on large angular scales. From Fig. 4, we see that many of the collective alignment axes in the case of varying l_{min} settled in the Galactic plane. Correspondingly, in the right-hand panel of Fig. 10, we see that the distribution of the HSIPs quantified by the *AD* statistic is very high compared to its expectation in the same multipole range, in the varying l_{min} case.

The *p*-values of the *AD* statistic for the *Planck* 2015 `Commander` map derived HSIPs as a function of l_{max} are shown in the left-hand panel of Fig. 11. The significances of the *AD* statistic for even and odd multipole PEV HSIPs are computed separately, and are shown in black and red solid lines with square and circle point types, respectively.

The AD statistic gives independent confirmation that the odd multipole PEV alignments are anomalous on large angular scales. Significance exceeding 2σ confidence level is found for $l_{max} = 9$, 19, 23 and 25, which are found to have high values for *AD* statistic from the left-hand plot of Fig. 10. The even-multipole PEV HSIPs show no significant signal of differing from the isotropic null distribution in this analysis, consistent with the finding from preceding section. Thus there are some anomalous alignments among odd multipole anisotropy axes on large angular scales represented by their PEVs that are resulting in the high significance of our test statistic. Owing to the highly deviant *AD* statistic in the varying l_{min} case, the *AD* statistic is found to be anomalous for the same range of multipoles. The *p*-value plot for the same is shown in right-hand panel of

Fig. 11, which follows a trend similar to the significances found in Fig. 5.

5 CONCLUSIONS

We have compared alignment statistics of parity even and odd multipoles with several independent methods. We used the clean CMB signal estimate from *Planck* 2015 data obtained using the `Commander` algorithm. Analysis was restricted to the first 60 multipoles, i.e. $l = [2, 61]$. Power tensor and Alignment tensor statistics were used to probe the alignments of even and odd parity multipoles, separately.

We studied the data in several ways. The collective alignment axes of even and odd multipoles show different behaviours. The anisotropy axes of even-parity multipoles from large angular scales are broadly clustered near the direction of the CMB dipole. The anisotropy axes of odd multipoles are much less concentrated, but are significantly directional as quantified by Alignment entropy.

We constructed cumulative statistical measures that fixed the lower limit $l_{\rm min} = 2$, while varying the upper limit to reach $l_{\rm max} = 61$. The Alignment entropy, S_X, of even-parity multipoles was as expected from an uncorrelated isotropic distribution. The odd-parity multipole S_X was unusually small on large angular scales with significance exceeding 2σ magnitude. As $l_{\rm max}$ was increased above $l_{\rm max} \sim 27$ the significance disappeared, apparently by dilution in the larger set. This significance nevertheless disappears by ignoring the first few multipoles. A similar effect was seen in studying even–odd multipole power asymmetry, using the *WMAP* 7 yr temperature power spectrum (Aluri & Jain 2012). To understand the alignment preferences of small angular scales in the range being studied, we fixed the upper limit at $l_{\rm max} = 61$ while varying the lower limit $l_{\rm min}$. A regime of multipoles with small S_X at 2σ or more significance for odd-parity multipoles was observed, with lowest p-value for S_X occurring at $l_{\rm min} \gtrsim 26$. The two different effects from varying $l_{\rm min}$ and $l_{\rm max}$ analysis in a single data set pose a puzzle. The resolution may involve two different populations separated by a middle range of $l \sim 27$, with each population diluting a distinctive signal of the other when populations are mixed. The observation that the axes of the $l > 27$ set settled at the Galactic plane may be an indication of a residual Galactic bias in this subset.

These results are further tested against potential residual contamination in the full sky map by excising different fractions of the sky, and then inpainting the masked region. The odd-multipole common axes are stable against Galactic cuts up to excluding (and then inpainting) 10 per cent of the sky, whereas the even multipoles are found to be sensitive to Galactic cuts.

An independent statistic was used to dissect the cumulative statistical studies. The HSIPs are rotationally invariant statistics with an analytic isotropic null distribution. The distribution of the data compared to the HSIP null was computed using AD test statistic. For the odd multipole PEVs, the AD statistic for the data HSIPs shows a significance similar to that found using the Alignment entropy method. The AD method pinpoints $l_{\rm max} = 9$, 19, 23 and 25 as containing unusual alignments that are rendering the AD statistic anomalous at a significance of 2σ or more.

Interestingly, we find that the even mirror parity axis from the *Planck* 2015 results, and the even-multipole common axes from large angular scales computed here, broadly point in the CMB dipole direction. Likewise, the odd mirror parity axis from the *Planck* 2015 analysis and the odd parity low-l hemispherical power asymmetry axis fall in the region spanned by the odd multipole alignment axes. From these observations, we speculate that these anomalous axes may have a common origin in their peculiar parity (a)symmetry properties.

We plan to investigate these speculations more in a later work.

ACKNOWLEDGEMENTS

We acknowledge the use of freely available HEALPIX[8] (Gorski et al. 2005) package and ISAP software[9] in this work. Part of the results presented here is based on observations obtained with *Planck*,[10] an ESA science mission with instruments and contributions directly funded by ESA Member States, NASA, and Canada. We also acknowledge the use of *WMAP* data made available from Legacy Archive for Microwave Background Data Analysis[11] (LAMBDA) site that is a part of NASA's High Energy Astrophysics Science Archive Research Center (HEASARC). This research used resources of the National Energy Research Scientific Computing (NERSC) Center, a DOE Office of Science User Facility supported by the Office of Science of the U.S. Department of Energy under Contract No. DE-AC02-05CH11231.

PKA is funded by the post-doctoral fellowship program of the Claude Leon Foundation, South Africa at UCT. This work is based on the research supported by the South African Research Chairs Initiative of the Department of Science and Technology and the National Research Foundation (NRF) of South Africa as well as the Competitive Programme for Rated Researchers (Grant Number 91552) (AW). Any opinion, finding and conclusion or recommendation expressed in this material is that of the authors and the NRF does not accept any liability in this regard.

PKA also thanks Pankaj Jain for helpful exchanges on an earlier version of the paper. AW would like to thank David Spergel for helpful discussions on this work.

We thank the anonymous referee for a careful reading and helpful comments on our paper.

REFERENCES

Abramo L. R., Bernui A., Ferreira I. S., Villela T., Wuensche C. A., 2006, Phys. Rev. D, 74, 063506
Aiola S., Wang B., Kosowsky A., Kahniashvili T., Firouzjahi H., 2015, Phys. Rev. D, 92, 063008
Akrami Y., Fantaye Y., Shafieloo A., Eriksen H. K., Hansen F. K., Banday A. J., Górski K. M., 2014, ApJ, 784, L42
Aluri P. K., Samal P. K., Jain P., Ralston J. P., 2011, MNRAS, 414, 1032
Aluri P. K., Jain P., 2012, MNRAS, 419, 3378
Anderson T. W., Darling D. A., 1954, J. Am. Stat. Assoc., 49, 765
Ben-David A., Kovetz E. D., Itzhaki N., 2012, ApJ, 748, 39
Bennett C. et al., 2011, ApJS, 192, 17
Bennett C. L. et al., 2013, ApJS, 208, 20
Bernui A., 2008, Phys. Rev. D, 78, 063531
Bernui A., 2009, Phys. Rev. D, 80, 123010
Bernui A., Mota B., Reboucas M. J., Tavakol R., 2007, A&A, 464, 479
Bernui A., Oliveira A. F., Pereira T. S., 2014, JCAP, 10, 041
Bielewicz P., Eriksen H. K., Banday A. J., Gorski K. M., Lilje P. B., 2005, ApJ, 635, 750
Bobin J., Sureau F., Starck J.-L., 2016, A&A, 591, A50
Bohm G., Zech G., 2010, Introduction to Statistics and Data Analysis for Physicists. Verlag Deutsches Elektronen-Synchrotron, Hamburg, Germany

[8] http://healpix.jpl.nasa.gov/
[9] http://www.cosmostat.org/software/isap/
[10] http://www.esa.int/Planck
[11] https://lambda.gsfc.nasa.gov/product/map/dr5/

Copi C. J., Huterer D., Starkman G. D., 2004, Phys. Rev. D, 70, 043515
Copi C. J., Huterer D., Schwarz D. J., Starkman G. D., 2006, MNRAS, 367, 79
Copi C. J., Huterer D., Schwarz D. J., Starkman G. D., 2015, MNRAS, 449, 3458
Cruz M., Tucci M., Martinez-Gonzalez E., Vielva P., 2006, MNRAS, 369, 57
Cruz M., Cayon L., Martinez-Gonzalez E., Vielva P., Jin J., 2007, ApJ, 655, 11
Cruz M., Vielva P., Martinez-Gonzalez E., Barreiro R. B., 2011, MNRAS, 412, 2383
de Oliveira-Costa A., Tegmark M., 2006, Phys. Rev. D, 74, 023005
de Oliveira-Costa A., Tegmark M., Zaldarriaga M., Hamilton A., 2004, Phys. Rev. D, 69, 063516
Eriksen H. K. et al., 2004a, ApJS, 155, 227
Eriksen H. K., Hansen F. K., Banday A. J., Gorski K. M., Lilje P. B., 2004b, ApJ, 609, 1198
Eriksen H. K., Banday A. J., Gorski K. M., Hansen F. K., Lilje P. B., 2007, ApJ, 660, L81
Eriksen H. K., Jewell J. B., Dickinson C., Banday A. J., Górski K. M., Lawrence C. R., 2008, ApJ, 676, 10
Finelli F., Gruppuso A., Paci F., Starobinsky A. A., 2012, JCAP, 07, 049
Flender S., Hotchkiss S., 2013, JCAP, 09, 033
Górski K. M., Hivon E., Banday A. J., Wandelt B. D., Hansen F. K., Reinecke M., Bartelmann M., 2005, ApJ, 622, 759
Gruppuso A., Burigana C., 2009, JCAP, 08, 004
Gruppuso A., Finelli F., Natoli P., Paci F., Cabella P., de Rosa A., Mandolesi N., 2011, MNRAS, 411, 1445
Gurzadyan V. G., Ghahramanyan T., Kashin A. L., Khachatryan H. G., Kocharyan A. A., Kuloghlian H., Vetrugno D., Yegorian G., 2009, A&A, 498, L1
Hajian A., Souradeep T., 2003, ApJ, 597, L5
Hansen F. K., Banday A. J., Gorski K. M., Eriksen H. K., Lilje P. B., 2009, ApJ, 704, 1448
Hansen M., Frejsel A. M., Kim J., Naselsky P., Nesti F., 2011, Phys. Rev. D, 83, 103508
Kim J., Naselsky P., 2010, ApJ, 714, L265
Kim J., Naselsky P., 2011, ApJ, 739, 79
Land K., Magueijo J., 2005a, Phys. Rev. D, 72, 101302(R)
Land K., Magueijo J., 2005b, Phys. Rev. Lett., 95, 071301
Lew B., 2008, JCAP, 09, 023
Maris M., Burigana C., Gruppuso A., Finelli F., Diego J. M., 2011, MNRAS, 415, 2546
Nadathur S., Lavinto M., Hotchkiss S., Rasanen S., 2014, Phys. Rev. D, 90, 103510
Naselsky P., Hansen M., Kim J., 2011, JCAP, 09, 012
Naselsky P., Zhao W., Kim J., Chen S., 2012, ApJ, 749, 31
Notari A., Quartin M., 2015, JCAP, 06, 047
Paci F., Gruppuso A., Finelli F., Cabella P., de Rosa A., Mandolesi N., Natoli P., 2010, MNRAS, 407, 399
Planck Collaboration IX, 2016, A&A, 594, A9
Planck Collaboration X, 2016, A&A, 594, A10
Planck Collaboration XII, 2016, A&A, 594, A12
Planck Collaboration XVI, 2016, A&A, 594, A16
Planck Collaboration XXIII, 2014, A&A, 571, A23
Polastri L., Gruppuso A., Natoli P., 2015, JCAP, 04, 018
Quartin M., Notari A., 2015, JCAP, 01, 008
Ralston J. P., Jain P., 2004, IJMPD, 13, 1857
Rassat A., Starck J.-L., 2013, A&A, 557, L1
Rassat A., Starck J.-L., Paykari P., Sureau F., Bobin J., 2014, JCAP, 08, 006
Rath P. K., Jain P., 2013, JCAP, 12, 014
Reed M., Simon B., 1972, Methods of Modern Mathematical Physics – 1. Functional Analysis. Academic Press, New York
Samal P. K., Saha R., Jain P., Ralston J. P., 2008, MNRAS, 385, 1718
Samal P. K., Saha R., Jain P., Ralston J. P., 2009, MNRAS, 396, 511
Santos L., Villela T., Wuensche C. A., 2012, A&A, 544, A121
Sarkar D., Huterer D., Copi C. J., Starkman G. D., Schwarz D. J., 2011, Astropart. Phys., 34, 591

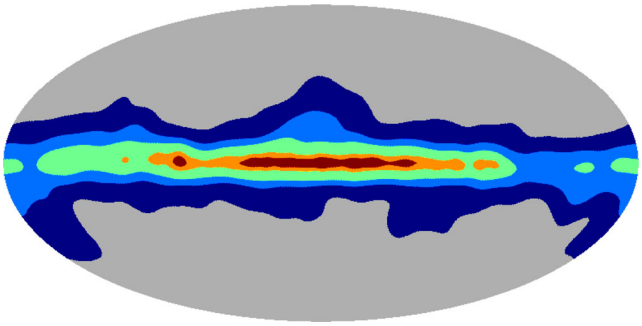

Figure A1. Foreground exclusion masks that are applied to test the stability of the collective alignment axes. From red to deep blue they progressive exclude 1 per cent, 3 per cent, 10 per cent, 20 per cent and 30 per cent of the sky. We used the freely available ISAP software to inpaint the masked region.

Schwarz D. J., Starkman G. D., Huterer D., Copi C. J., 2004, Phys. Rev. Lett., 93, 221301
Schwarz D. J., Copi C. J., Huterer D., Starkman G. D., 2016, CQG, 33, 184001
Slosar A., Seljak U., 2005, Phys. Rev. D, 70, 083002
Starck J.-L., Rassat A., Fadili M. J., 2013, A&A, 550, A15
Vielva P., Martinez-Gonzalez E., Barreiro R. B., Sanz J. L., Cayon L., 2004, ApJ, 609, 22
Wiaux Y., Vielva P., Martinez-Gonzalez E., Vandergheynst P., 2006, Phys. Rev. Lett., 96, 151303
Zhao W., 2014, Phys. Rev. D, 89, 023010

APPENDIX A: STABILITY OF ALIGNMENT AXES

Here we probe the stability of the even/odd multipole alignment axes using different foreground exclusion masks. We used *Planck* 2015 HFI masks with varying sky fractions, that are provided along with the second public release of *Planck* data.[12] The respective sky fractions of the masks used are 1 per cent, 3 per cent, 10 per cent, 20 per cent and 30 per cent. The excluded regions corresponding to these masks are shown in Fig. A1.

We used these masks at their native resolution of HEALPIX $N_{\rm side} = 2048$ on the *Planck* 2015 `Commander` CMB temperature map that is also made available at the same resolution. The masked CMB map is then inpainted using the freely available ISAP software[13] (see Starck et al. 2013). We used the default settings of the `mrs_alm_inpainting` facility of ISAP to inpaint the CMB sky.

Following the same procedure as described in the main analysis, the inpainted CMB map is then downgraded to $N_{\rm side} = 256$ and simultaneously smoothed to have a beam resolution of FWHM $= 1^\circ$ Gaussian beam.

The common alignment axes of even and odd multipole PEVs from masking and inpainting 3 per cent, 10 per cent and 20 per cent of the CMB sky are shown in Fig. A2. Here we performed a qualitative analysis only. By visual inspection we see that the odd multipole alignment axes are broadly stable up to 10 per cent of the sky being masked and inpainted. However, the even-multipole PEV alignment axes steadily drift towards Galactic plane in the varying $l_{\rm max}$ and move towards the poles in the case of varying $l_{\rm min}$. Applying Galactic cuts with 20 per cent or more masking fraction (followed by inpainting the masked sky) is found to destroy the alignment patterns seen otherwise.

[12] http://irsa.ipac.caltech.edu/data/Planck/release_2/ancillary-data/
[13] http://www.cosmostat.org/software/isap/

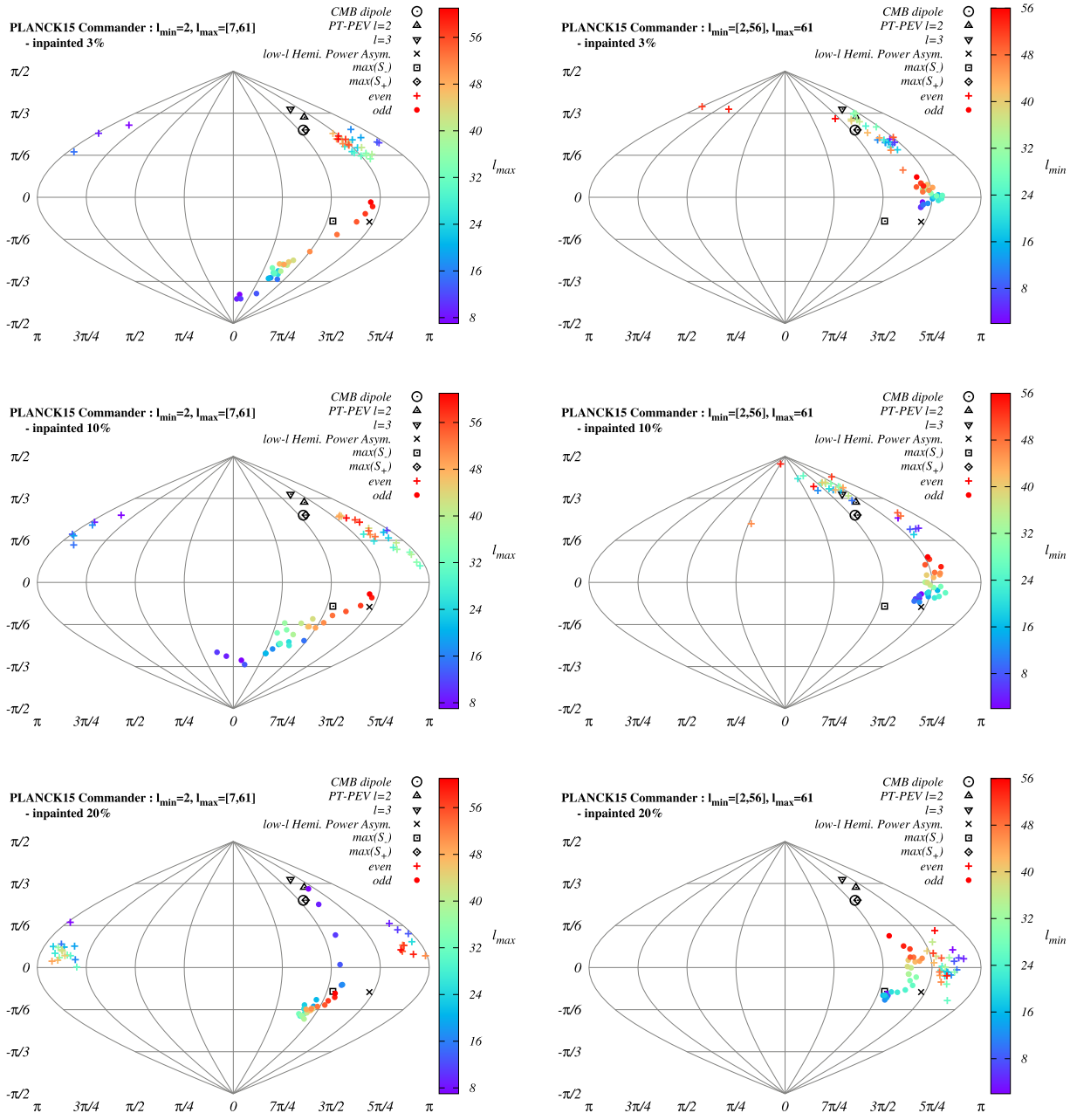

Figure A2. Common alignment axes obtained after applying Galactic masks with different sky fraction and inpainting using ISAP. The varying $l_{\rm max}$ and $l_{\rm min}$ cases are shown in the *left-hand* and *right-hand* columns, respectively, for masking fractions of 3 per cent, 10 per cent and 20 per cent of the sky. By excluding 20 per cent or more sky fraction (and then inpainting), the broad orientations of the common alignment axes disappears.

APPENDIX B: THE ISOTROPIC NULL *HSIP* DISTRIBUTION

Let $|\tilde{e}_l\rangle$ be a random eigenvector from an isotropic distribution. Since eigenvectors have no magnitude and no sign, $|\tilde{e}_l\rangle$ is equivalent to the rank-one projector $\Pi_l = |\tilde{e}_l\rangle\langle\tilde{e}_l|$. Consider the distribution of $x = Tr\{\Pi_l^\dagger \Pi_{l'}\} = \langle\tilde{e}_l|\tilde{e}_{l'}\rangle^2$ (for all $l \neq l'$). Choose coordinates where the first instance $|\tilde{e}_1\rangle$ is along the z axis, so that $\langle\tilde{e}_l|\tilde{e}_1\rangle = \cos\theta_l$. In an isotropic ensemble the distribution of $\cos\theta_l$ is constant over the range $-1 \leq \cos\theta \leq 1$ as shown by the solid angle measure $\mathrm{d}\Omega_l = \mathrm{d}\cos\theta_l\,\mathrm{d}\phi_l$. Averaging over all cases we can drop the index l. For each $x = \cos^2\theta$ there are two signs of $\cos\theta$. The distribution of x over the range $0 \leq x \leq 1$ is then

$$f(x) = \frac{\mathrm{d}N}{\mathrm{d}x} = 2\frac{\mathrm{d}N}{\mathrm{d}\cos\theta}\left|\frac{\mathrm{d}\cos\theta}{\mathrm{d}x}\right| = \frac{2}{2}\frac{\mathrm{d}\sqrt{x}}{\mathrm{d}x} = \frac{1}{2\sqrt{x}}.$$

The same result comes from $f(x) = (2\pi/4\pi)\int_{-1}^{1}\mathrm{d}\cos\theta\;\delta(\cos^2\theta - x)$, accounting for two solutions of the delta function.

This paper has been typeset from a TEX/LATEX file prepared by the author.